

An ultrafine sea-salt flux from breaking waves: Implications for cloud condensation nuclei in the remote marine atmosphere

Antony D. Clarke,¹ Steven R. Owens,² and Jingchuan Zhou¹

Received 5 August 2005; revised 6 November 2005; accepted 7 December 2005; published 16 March 2006.

[1] Sea-salt aerosol (SSA) is an important constituent of natural marine aerosol to which anthropogenic aerosols must be compared when assessing their climatic influence. Size distributions of particles, produced by bubbles from coastal oceanic breaking waves, were found to have sizes as small as 0.01 μm , with 60% smaller than 0.1 μm diameter. The thermal stability of these particles and their growth factor measured under increasing humidity indicate that most are sea salt. These SSA size distributions were used in conjunction with the measured number flux for bubbles from coastal breaking waves to develop a new sea-salt source function. This source function and the associated SSA flux compare favorably with previously published estimates available for sizes larger than 0.5 μm but extend the source function down to much smaller sizes. When this SSA flux is applied to oceanic whitecaps that have a highly nonlinear dependence on wind speed, it implies strong regional and temporal differences in the open ocean surface number flux. In marine regions with little continental impact we estimate that this SSA flux can contribute $\sim 5\text{--}90\%$ of the marine cloud condensation nuclei (CCN), with the rest accounted for by the flux of aerosol entrained from the free troposphere. These two fluxes are large enough to account for commonly observed aerosol and CCN concentrations in the clean MBL without requiring a nucleation source in the MBL. These observations have significant implications for modeling marine aerosol concentrations and evolution.

Citation: Clarke, A. D., S. R. Owens, and J. Zhou (2006), An ultrafine sea-salt flux from breaking waves: Implications for cloud condensation nuclei in the remote marine atmosphere, *J. Geophys. Res.*, *111*, D06202, doi:10.1029/2005JD006565.

1. Introduction

[2] Sea-salt aerosol (SSA) produced from breaking waves (BW) influence marine boundary layer (MBL) heterogeneous chemistry, atmospheric optics and cloud physics. Dry SSA sizes between 0.1 μm and 100 μm originate as droplets ejected from bursting bubbles [Blanchard and Woodcock, 1957] and have been the focus of investigations for decades [e.g., Woodcock, 1950]. They constitute the largest global production rate of aerosol mass [Warneck, 1988] and dominate visibility reduction in the clean marine boundary layer (MBL) free of continental influence [Quinn *et al.*, 1998]. SSA play important roles in air-sea exchange, the scattering of light in the MBL, influences MBL aerosol chemistry [Sievering *et al.*, 2004] and affects the microphysical properties of marine clouds by acting as cloud condensation nuclei (CCN). Understanding the magnitude and variation in this natural source is necessary in order to better assess anthropogenic and continental impacts and to

improve interpretation of satellite retrievals and modeling efforts used to resolve the relative influence of continental and anthropogenic sources. However, in spite of decades of studying the processes and properties that govern the size and concentration of SSA, their size-resolved flux remains uncertain to about an order of magnitude [Lewis and Schwartz, 2004]. During this time the early notion that CCN in the MBL were dominated by SSA was replaced by the arguments that other aerosol such as sulfate were the primary contributors. Here we characterize contributions of both aerosol types to MBL aerosol and CCN in terms of their fluxes.

[3] Physical processes at the ocean surface eject sea-salt aerosol into the MBL. The most important are indirect mechanisms (bubble mediated) resulting from the entrainment of air by a BW, to produce small film and jet droplets. The production rate or source function for these droplets is often estimated to be directly proportional to the fractional whitecap coverage [Monahan *et al.*, 1986]. A collection of source functions reviewed by Andreas [1998] revealed that the estimated volume fluxes vary by 6 orders of magnitude. More recent assessments have reduced variations in the number flux to within about an order of magnitude [Lewis and Schwartz, 2004] for sizes below 10 μm . When restricted to the so-called “whitecap method” described here, these authors argue the uncer-

¹School of Ocean and Earth Science and Technology, University of Hawaii, Honolulu, Hawaii, USA.

²Department of Meteorology, University of Hawaii, Honolulu, Hawaii, USA.

tainty to be about a factor of 7 on the basis of the results of ten studies.

[4] We assume here that bubbles produced from coastal BW can provide a suitable surrogate for those from common open ocean BW. However, the formation and evolution of bubbles from BW is dynamic, complex and highly intermittent. Actual measurements of open ocean subsurface bubble concentrations vary by well over an order of magnitude [Lewis and Schwartz, 2004, and references therein], and limited measurements of surf zone concentrations tend to be higher than open ocean concentrations. However, the observed BW bubble spectrum is shown to be similar under open ocean, surf and laboratory conditions [Deane and Stokes, 2002]. Regardless of the details of bubble production and below-surface bubble concentrations for these different wave types and environments, in this paper we assume that the aerosol flux produced from a unit of bubble covered ocean surface is the same for coastal and open ocean conditions. We also assume that the open ocean aerosol flux scales with bubble coverage under increasing wave height and wind speed based upon the parameterization in terms of white cap coverage [Monahan *et al.*, 1986]. We recognize that large-scale differences in water mass characteristics such as temperature, salinity and organic films, etc., are likely to exert influences on production in ways that remain uncertain [Lewis and Schwartz, 2004], but these effects are not considered here.

[5] The SSA volume or mass concentration is dominated by larger sizes that can be measured reasonably well by chemical and other techniques. However, knowledge of the number flux of SSA has evolved more slowly because, until recently, most techniques fail to distinguish SSA from other aerosol present at dry diameters below $\sim 0.5 \mu\text{m}$. Even so, bubblers and plunging water (NaCl solutions) have been shown to yield particles smaller than $0.04 \mu\text{m}$ diameter [Cipriano *et al.*, 1987], and some TEM analysis of remote oceanic impactor samples [Murphy *et al.*, 1998] identify SSA down to $0.06 \mu\text{m}$. This was recently supported by a wind-driven turbulent upward flux of accumulation mode marine aerosol measured in the Arctic [Nilsson *et al.*, 2001], where a mode smaller than $0.1 \mu\text{m}$ was detected. Hygroscopic analysis of these [Zhou *et al.*, 2001] identified a fraction with properties similar to SSA down to diameters of $0.035 \mu\text{m}$. On the basis of indirect measurements, a source function has been inferred and modeled by extending the Monahan *et al.* function from $0.4 \mu\text{m}$ down to $0.02 \mu\text{m}$ [Gong, 2003]. More recent laboratory measurements in surrogate seawater confirmed significant particle production for sizes as small as $0.02 \mu\text{m}$ [Martensson *et al.*, 2003].

[6] Here we use the size distributions and the effective SSA flux measured directly from coastal BW to demonstrate that the number flux of SSA into the MBL can be dominated by sizes less than $0.1 \mu\text{m}$ and that SSA can be a significant, and at times primary, source of CN and CCN to the unpolluted marine atmosphere. Sizes above a few μm are less well characterized here and can compose most of the sea-salt mass, but we show that these have negligible influence on the number flux. We will demonstrate that after removing open ocean concentrations the excursions in coastal aerosol number concentrations can be quantitatively linked to the surface bubble coverage from BWs. Characterization of the height and vertical gradient in this coastal

aerosol field will be used to establish the sea-salt number flux for 100% bubble coverage. In this paper we assume this flux applies for 100% bubble coverage over the open ocean and demonstrate that it compares well with other oceanic flux estimates.

[7] We next use this open ocean sea-salt flux along with the aerosol flux estimated to be entrained from the free troposphere, FT, in order to gauge the relative contribution from these two sources. These fluxes establish the MBL CN and CCN concentrations when they are combined with processes that influence removal and evolution of these aerosol. A volatile monomodal aerosol formed in the FT appears common above the MBL inversion [Clarke *et al.*, 1999]. Pioneering measurements of CCN in remote marine regions [Dinger *et al.*, 1970] identified refractory sea salt in the lower few kilometers and showed that 50% of CCN were also volatile and not sea salt. They also showed that the fraction of volatile CCN increased with altitude and these were completely volatile above the inversion in subsiding air masses. In the latter part of this paper we will examine the implications of the size distributions and fluxes of sea salt from the surface and the entrainment flux of sulfate from the FT and show how both sources can be important for MBL CN and CCN. Although we recognize that the fluxes idealized here and the more commonly measured MBL concentrations are not directly related without consideration of loss terms, we will also present some measured concentration data that is consistent with the fluxes described here.

2. SSA Measurements

[8] The University of Hawaii Coastal Aerosol Facility at Bellows Air Force Station (BAFS, $21^{\circ}21'N$, $157^{\circ}42'W$) has a 20 m tower ~ 20 – 30 m from waters edge and sampling inlets are oriented into the prevailing trade winds. The bottom slopes gradually from the waters edge for ~ 35 m to where the water depth is 1.5 – 2 m in the lagoon area. This site was characterized for the Shoreline Environment Aerosol Study (SEAS) and details of this sampling facility, coastal setting and environmental issues are discussed at length elsewhere [Clarke and Kapustin, 2003] and will not be discussed here. A complete description of the sampling method and instrumentation used during SEAS to establish the SSA size distribution and loss corrections is similarly given by Clarke *et al.* [2003]. A brief summary follows.

[9] Nominally “dry” ($RH = 40\%$) particle size distributions covering $0.01 \leq D_p \leq 8 \mu\text{m}$ ($146 D_p$ channels) were obtained by combining data collected from a radial differential mobility analyzer (DMA), optical particle counter (OPC, LAS-X, PMS Boulder CO) and an aerodynamic particle sizer, APS (TSI, 3321). The DMA and OPC included options for sampling aerosol at ambient or 360°C to identify volatile and residual refractory sizes [Clarke, 1991]. A tandem DMA (TDMA) and humidified TDMA were also used to examine the thermal and humidification response of selected sizes. Two condensation nuclei (CN) counters (TSI 3760) were used to measure aerosol number concentrations. One operated at ambient temperature (CNcold) while the other collected data after heating the sampled volume to 360°C (CNhot) to vaporize volatile components such as sulfates, leaving only thermally

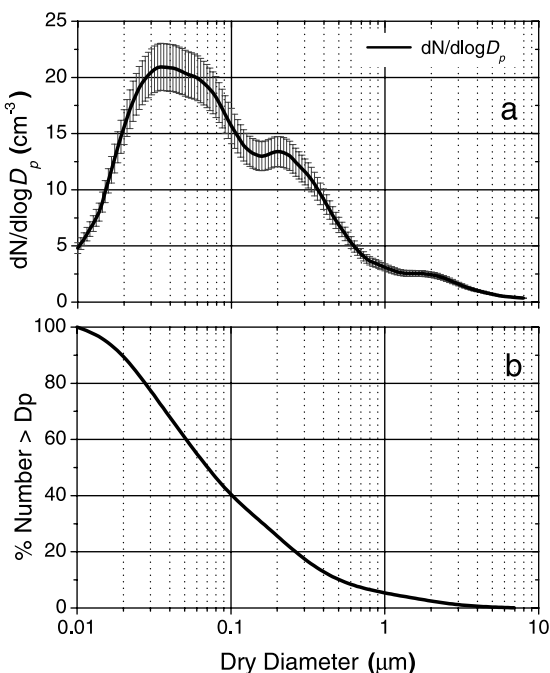


Figure 1. (a and b) Mean SEAS refractory number distribution from BW reveals that the majority of aerosols from BWs are $\leq 0.1 \mu\text{m}$, while particles $> 0.5 \mu\text{m}$, which scatter light most efficiently, contribute little to the total number concentration.

stable particles with a refractory component (e.g., sea salt or soot). Hereafter, these higher-temperature measurements will be referred to as heated or hot. Scattering coefficients (σ_{sp}) at the tower were measured by a three-wavelength integrating nephelometer (TSI 3563) over an angular range of 7° – 170° .

[10] An important aspect of the SEAS measurements involves them being taken from inlets placed at 5, 10 and 20 m on the tower. Sampling was cycled through each inlet at regular intervals to reveal the temporal and vertical variation in marine aerosol properties. The data at the top of the tower did not reveal the impact of coastal breaking waves while at 10 m a weak influence was occasionally detected. The data at 5 m was continuously influenced by BW aerosol. Hence, by differencing the 5 m and 20 m measurements, the contributions from BW (Figure 1) were isolated from the background aerosol [Clarke *et al.*, 2003]. It is the mean average “shape” of the BW distributions established during SEAS that is used here to determine the BW particle flux after being scaled by the number concentrations determined here from BW bubble coverage.

[11] Size distributions were measured using the DMA and OPC equipped to heat aerosol to 300° – 360°C and drive off volatile species (e.g., sulfate) common to clean marine regions [Clarke, 1991] and were shown to be dominated by volatile sulfates. Application of volatility to explore properties of aerosol and CCN began with the work of Twomey [1968] and other pioneering studies [Dinger *et al.*, 1970]. Although some organic material may exhibit volatility behavior similar to sulfates in the MBL, measurements with an Aerodyne mass spectrometer sampling air advected over the North Pacific found organic species were only $\sim 15\%$ of

the observed sulfate aerosol mass in the accumulation mode [Allan *et al.*, 2004]. Different temperatures and instruments have been used on various experiments but in regions free of pollution or dust, the nonvolatile “refractory” component is generally SSA with a mass distribution that peaks at sizes above $1 \mu\text{m}$. However, the “tail” extending down to $0.1 \mu\text{m}$ has little mass but has been shown to include the highest SSA number concentrations [Clarke and Porter, 1993; O’Dowd and Smith, 1993].

[12] Apart from the measurements outlined above, additional SSA concentration profiles were measured over the beach upwind of the tower in September 2004. These were required in order to establish a link between concentration measurements made on the tower during SEAS to the full gradient in the BW aerosol profile over the beach. This evaluation employed an A-frame ladder facing the onshore flow about half way between the tower and shoreline. In conjunction with concurrent measurements on the tower, the frame supported an inlet that could be varied between 1 and 4 m to establish the near-surface unperturbed vertical gradient from coastal BWs. In addition to CN, concurrent values for σ_{sp} were measured on the beach using a single wavelength nephelometer (Radiance Research, M903).

[13] Later we also discuss separate data from DMA thermal analysis that distinguished SSA diameters down to $0.02 \mu\text{m}$ in the equatorial zone at Christmas Island (CI; 2°N , 157°W) in 1994 [Clarke *et al.*, 1996] and some aircraft measurements made during the Pacific Exploratory Missions–Tropics (PEM-T) [Clarke *et al.*, 1999]. Measurements at both SEAS and CI sites were made from a 20 m coastal tower ~ 30 m from the surf line. This allowed the characterization of remote oceanic aerosol as well as contributions from near-surface coastal BW [Clarke *et al.*, 2003]. We note here that there was an incorrect statement in this referenced paper regarding the charging distribution for our RDMA where we stated [Clarke *et al.*, 2003, p. 1367] “The RDMA places a Boltzmann charge distribution on the aerosol . . .”. In this previous work and in this paper a bipolar neutralizer containing 210 Po source was employed to charge the aerosol sample. Our program actually calculates the charge probability using Fuchs’ theory [Fuchs, 1963] and Wiedensohler’s coefficients [Wiedensohler, 1988] for specified particle diameter at measured temperature and pressure.

3. Sea Salt From Breaking Waves

[14] The aerosol data analyzed here directly reflects the details of the BW evolution as illustrated in Figure 2. Initially the waves break and plunge to produce the wave front that generates the leading concentration of the BW aerosol plume. As the waves move to shore the width of the BW front diminishes. The area with bubbles behind the BW front increases while the bubble surface coverage decreases. Eventually the resulting aerosol flux goes through a maximum and decreases. Typical wave speeds for the data discussed here were $\sim 1.6 \text{ ms}^{-1}$ while winds at 10 m altitude were $\sim 7 \text{ ms}^{-1}$, resulting in about a 5–10 s transit time to the tower. Here we assume negligible particle loss because deposition velocities for the size range that dominate aerosol number are very low. This plume from each BW is produced continuously over the time it takes the

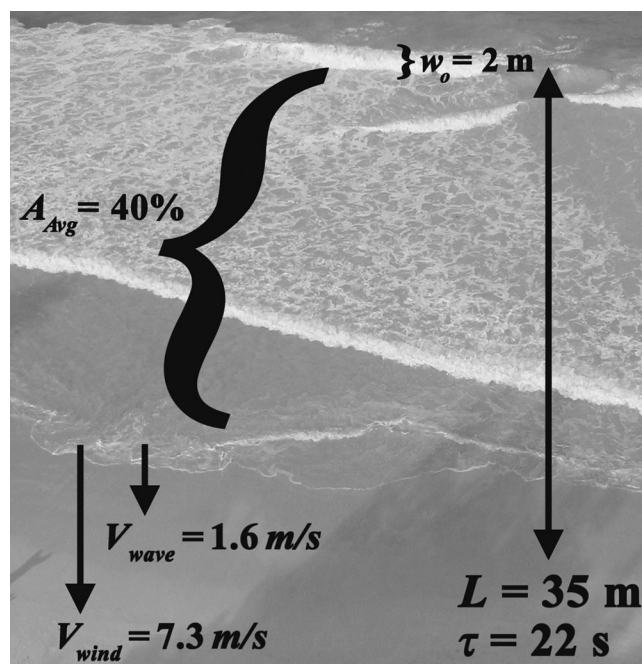


Figure 2. Photograph of beach and incoming BWs at BAFS with overlay of some variables used to establish the source function.

wave to reach the shore (~ 20 s) to yield concentrations at the tower that vary over a similar time period (Figure 3a). Generally a dominant wave is clearly resolved on these timescales (e.g., 4 successive peaks in 225 to 310 s period) but multiple waves are also evident in the merging of some peaks.

[15] Concentrations of particles from BW measured at the tower depend upon the bubble coverage caused by the BWs, the dilution arising from the wind over the bubble region, the influences upon vertical mixing over the distance to the tower, obstacles to flow near the tower and more subtle effects of wind direction, swell, tide, etc. [Clarke and Kapustin, 2003]. Unlike open ocean BW that experience a higher drag from increasing wind speed leading to an increased aerosol flux and higher atmospheric concentrations, here the coastal BW are mechanically forced by interactions with topography and increasing wind actually lowers concentrations from coastal BW through dilution [Clarke and Kapustin, 2003].

[16] Our measurements of heated CN and light scattering at the tower resolve the influence of individual BW events. Figure 3a shows a time series of well-defined BW events observable in corresponding CNhot and σ_{sp} excursions obtained after subtracting the background values measured at 20 m. The wider overlapping peaks (at 350–425 s) are a result of production from multiple BWs in close succession (Figure 2). Excursions in CNhot and σ_{sp} (Figure 3b) are highly correlated ($r = 0.95$). This correlation is significant because it confirms the small aerosol ($D_p \leq 0.1 \mu\text{m}$) that dominate excursions in number (see Figure 1) and the larger aerosol ($0.5 \leq D_p \leq 10.0 \mu\text{m}$) that dominate σ_{sp} are both produced concurrently and proportionally across the entire distribution as a result of

the bubble bursting process. Note that particles that dominate σ_{sp} are particles larger than $0.5 \mu\text{m}$ and represent only 12% of the total number (Figure 1b).

[17] This 9 minute data is representative and similar analysis for several other measurement periods conducted over a 24 hour period result in $r = 0.85$. We have consistently observed nearly equal excursions in both CNhot and CNcold in other coastal regions. This would be expected if aerosol variability is driven by variations in residual refractory aerosol mixed with a volatile mode that is more stable [Clarke et al., 2003], as discussed later. This behavior also suggests that all refractory sizes from BW shown in Figure 1 could be SSA [Clarke et al., 2003] with the majority having sizes smaller than $\leq 0.1 \mu\text{m}$. Repeated recent measurements (not shown) of excursions in light scattering and CNhot measured on ship for varying winds over the open ocean around Hawaii exhibit a similar high correlation. The slope of the relation appears to depend upon distance from the BW source with less scattering per change in CNhot at greater source distances, as expected for a more rapid removal of the fewer coarse particles that dominate scattering compared to the majority that dominate refractory number. This open ocean correlation also implies similar production from bubbles for both coastal and open ocean BWs, as assumed in this paper.

3.1. Ultrafine Sea Salt

[18] The small refractory particles are clearly produced by breaking waves and highly correlated with the larger SSA that dominate the light scattering (Figure 3b). Although it is well known that larger sizes produced by BWs are sea salt it does not follow that the smaller sizes are necessarily SSA. Hence we undertook two experiments in 2004 to better identify these small sizes. We first carried out concurrent experiments with other investigators using a DMA and a flame photometric aerosol sodium detector (ASD). Initial studies with a prototype ASD during SEAS

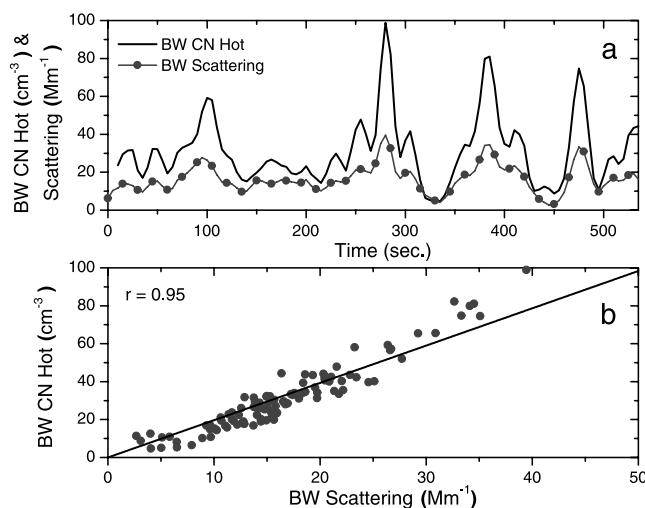


Figure 3. (a) Time series of σ_{sp} and CNhot at 5 m produced from BW after subtracting oceanic background values recorded at 20 m on the tower. (b) Linear regression of typical conditions linking σ_{sp} and CNhot for BW during SEAS.

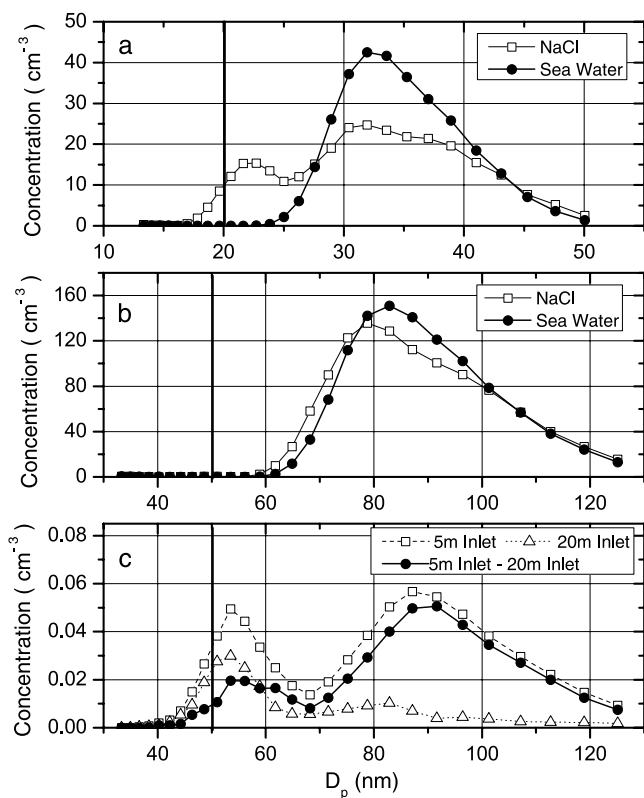


Figure 4. Plots for humidified TDMA aerosol at 76% RH. (a) Size of a selected dry 20 nm mode aerosol after humidification for prepared NaCl and for coastal seawater. (b) Same as Figure 4a only for selected 50 nm size. (c) Growth of humidified ambient aerosol selected at 50 nm for background aerosol (20 m inlet) and coastal aerosol (5 m inlet) and their difference due to BW.

[Campuzano-Jost *et al.*, 2003] revealed that the pulses from BW (e.g., Figure 3a) were made up of SSA down to the ASD instrument detection limit of $0.3 \mu\text{m}$. A repeat study in 2004 with an improved ASD confirmed similar behavior down to a detection limit of $0.09 \mu\text{m}$ [Campuzano-Jost *et al.*, 2004]. Because sizes smaller than $0.09 \mu\text{m}$ are difficult to detect chemically, we also carried out humidification experiments using a Hygroscopic Tandem DMA (HTDMA) to characterize the hygroscopic properties of these smaller particles. For these studies the aerosol was heated to 300°C to drive off volatiles [Clarke, 1991]. The first DMA then selected a dry size and then the second DMA scanned the sizes after humidification in order to examine the associated size change. Because SSA has a characteristic size change upon humidification [Swietlicki *et al.*, 2000; Zhou *et al.*, 2001], the HTDMA results can be compared to known SSA response to humidification.

[19] The thermal and environmental conditions experienced by our humidified HTDMA system limited our upper limit to $\sim 76\%$ RH and small thermal variations within the HTDMA commonly resulted in a small range of humidity experienced by the aerosol [Swietlicki *et al.*, 2000]. Consequently, the instrumental humidification response for known aerosol was first characterized for selected sizes of dry heated aerosol generated with a

bubbler. This was done for both a prepared pure NaCl solution and coastal seawater obtained from 25 cm below the surface at the BAFS site. Figure 4a reveals the humidified distributions observed by the second DMA for a dry 20 nm heated size mode selected by the first DMA. These show a predominant mode that increases by a factor of ~ 1.6 in size and a smaller mode with little change. The latter could occur if the upper limit of our HTDMA system that did not provide a high enough saturation for some of the smaller pure NaCl to grow while the sea salt includes some salts that can effloresce and grew more readily at lower RH. We have observed similar behavior in other humidified TDMA systems. The 50 nm sizes (Figure 4b) for both NaCl and SSA show similar growth with the SSA slightly greater. Both modes are consistent with the expected modal growth factor for SSA near 1.8 at 76% RH [Tang *et al.*, 1997].

[20] Growth measurements for selected sizes of the heated ambient coastal aerosol are shown in Figure 4c. These were more challenging to obtain and required several hours for a given selected size. The ambient heated aerosol was first sampled by our 10 l Lagged Aerosol Grab (LAG) chamber [Clarke *et al.*, 1998] to “grab” a 10 s sample of air that was then heated to 300°C prior to TDMA humidity analysis. Later the data were stratified to extract samples at 5 m on the tower taken near the peak of a wave event as detected by the CN counters (e.g., Figure 3). These were identified and accumulated over time to yield an average growth. Sampling was also cycled between 20 m and 5 m on the tower every half hour during the measurement period to obtain 20 m background data for comparison with the data at 5 m influenced by BW plumes. A similar number of humidified HTDMA distributions from 20 m on the tower, sampled closest in time to the BW samples from 5 m on the tower, were also averaged. These two resulting average humidified-growth curves were then subtracted to yield the humidified-growth curve representative of ambient BW aerosol (with background aerosol growth so removed).

[21] An example of this growth behavior for a selected size of 50 nm is shown for 5 m, 20 m and for their difference in Figure 4c. The difference plot clearly reveals that most 50 nm aerosol from BW have a growth factor near 1.8, as expected for SSA at $\sim 76\%$ RH. About 20% show little growth and we believe that some these are a result of uncertainty arising from the sequential sampling for this approach. Some may also be a result of humidity variations in the humidifier and the second DMA of 1 to 3% during this experiment. Because 76% RH is close to the deliquescence point of SSA these variations may result in some particles not growing. Of course, it is also possible that some heated BW aerosol at 50 nm include components that do not grow much (e.g., organic films) [Zhou *et al.*, 2001]. If so, some of the 5 m BW aerosol that exhibit little growth may also contribute to the oceanic background aerosol. However, we cannot rule out the possibility that those present in the low-growth mode for the BW are just a consequence of our humidification system being limited to $\sim 76\%$ RH.

[22] Consequently, we believe that these data confirm that from 80% up to possibly 100% of the 50 nm particles from

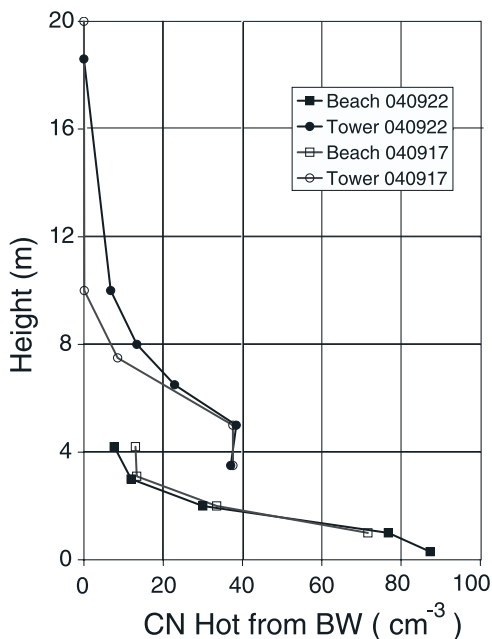


Figure 5. Vertical gradient in CNhot at BAFS for two days measured from 1 to 4 m above the beach (lower curves) and on the tower from 5 to 20 m (upper curves). Tower data <5 m are heavily influenced by BW while those at 20 m reflect background values.

BW have a humidity response consistent with their being predominantly SSA. Similar results were observed for other sizes but sizes smaller than 20 nm were difficult to assess given the decreasing concentrations in the BW size distribution (see Figure 1) and the lower charging efficiency in this range. We also note the similarity of our Figure 1 data to distributions from laboratory BW generated in artificial seawater [Martensson *et al.*, 2003]. Hence, in view of their refractory nature, the chemical identification of SSA down to 90 nm by the ASD and the TDMA humidity dependence of the smaller sizes, we conclude that the most of the particles from BWs are composed of SSA at least for diameters above ~30 nm. This implies that SSA diameters span 3 to 4 orders of magnitude and associated particle mass more than 10 orders of magnitude, arguably a greater range than any other natural aerosol.

[23] About half of the background refractory samples obtained from 20 m show little growth. This implies some background 50 nm sizes may be non-SSA aerosol. Similar low growth has been observed in unheated marine aerosol [Swietlicki *et al.*, 2000] but these were attributed to local pollution. Other refractory and nonhygroscopic aerosol in this size range has been identified as being organic [Leck and Bigg, 1999] from unusually productive surface waters in open leads in Arctic ice. Whether any similar organic sources exist over the predominantly oligotrophic central Pacific remains unknown. However, the size increase in those that do grow is slightly smaller than expected for NaCl and SSA in our system (Figure 4c). In any event, because these are subtracted from our 5 m measurements they do not impact our SSA analysis. Background CNhot concentrations measured at the top of the tower often range

between 50 and 100 cm^{-3} and for this measurement period were $\sim 65 \pm 5 \text{ cm}^{-3}$. These have been subtracted from all CNhot values shown here in order to leave only the contributions from coastal BWs.

3.2. Tower Data and the SSA Profile

[24] The SEAS measurements on the tower revealed the influence of BW consistently at 5 m, occasionally at 10 m and none at 20 m [Clarke *et al.*, 2003]. However, the 5 m data is sampled from a flow perturbed by the near-surface structures [Clarke and Kapustin, 2003]. Consequently, variations in the 5 m data correspond to the breaking wave SSA flux but do not represent data for an undisturbed aerosol profile. The turbulence generated near the tower tends to mix the high near-surface concentrations upward and increases 5 m tower values relative to the undisturbed profile over the beach. In order to relate the SEAS 5 m tower measurements to the flux of aerosol from the BW, it is essential to relate the typical excursions in concentrations measured on the tower under SEAS conditions to the unperturbed concentration profiles measured over the beach. It is the column integral over the unperturbed profile, after removal of the background concentrations measured at 20 m, that establishes the net BW particle flux.

[25] In order to establish the unperturbed concentration gradient generated by BWs we made careful profile measurements over the beach in 2004 on two days with favorable conditions similar to SEAS that included nearly stable 10 m winds in the 6–8 m/s range and with onshore flow near 70 ± 10 deg. Heated aerosol was concurrently sampled by CN counters on the tower and the beach through an identical 2 cm diameter tube. This was aspirated at ~ 10 lpm and could be raised and lowered to get profiles. Overall particle concentration losses in the tubes were measured to be $\sim 3\%$ and do not affect the observations made here. The maximum height profiles readily obtained over the beach were ~ 4 m and just sufficient to resolve the top of the BW plume.

[26] Figure 5 superposes two profiles of CNhot concentrations from BW aerosol made over the beach ~ 5 m from the water edge and those made on the tower ~ 20 m from the waters edge. Both days appear quite similar but with a few more frequent excursions of BW influence at 8 to 10 m on the tower on 22 September than on 17 September. However, on both days the concentration from BWs measured at 4 m over the beach has dropped to about one tenth of its near-surface value. This beach gradient agrees well with vertical LIDAR backscatter profiles made along the coast at BAFS during SEAS by Porter *et al.* [2003] and is also consistent with other reported beach profiles [Exton *et al.*, 1985; Sievering *et al.*, 2004]. It is less deep than a related SSA flux study [de Leeuw *et al.*, 2000] that inferred their profile from two points over an extended pier that had a longer fetch and was further downwind than the profile measured here. It was also noted that their unusually high estimate might be due to the influence of terrain.

[27] The concurrent tower profiles reveal very low BW contributions at 10 m. However, at 5 m the tower concentrations are similar to those measured at 2 m over the beach. Some of this increase at 5 m arises from additional vertical mixing during transit from the beach but most is a result of

vertical mixing driven by the complex flow around the 3 m structures at the base of the tower. Even so, the 5 m data from the tower exhibit a similar relationship to the profile on the beach for both days. An exponential fit was applied to the mean beach profiles shown in Figure 5 and integrated to estimate the mean total contribution from BWs. This resulting integral of effective concentration over the mean beach profile is ~ 1.5 times the mean BW concentration as measured at 5 m on the tower. We assume this relation is representative of the SEAS measurement period that was characterized by similar conditions. We employ this value in the flux determinations that follow as our “scale factor” required to relate our 5 m BW tower concentrations measured during SEAS to the mean effective concentration of the BW number profile over 4 m on the beach. On the basis of uncertainties in the height (± 0.6 m) of the beach profile “top” at the measured location, a tidal variation of about ± 0.5 m, possible variability in winds and turbulence, etc., we estimate the uncertainty in this value as 1.5 ± 0.3 .

3.3. Deriving the Sea-Salt Flux

[28] In deriving our SSA flux we make the assumption that the primary generation mechanism is the bursting of bubbles resulting from BWs. The sea-salt source function (S_{100}) is defined here as the number of sea-salt aerosols generated per unit area of ocean surface completely covered by bubbles (100% coverage) per unit time. We will show that this can be obtained from the mean of the fluctuations in refractory SSA aerosol measured as CNhot at the tower with background values removed (hereafter identified as C_s) when these are linked to the mean bubble coverage that gives rise to them. In order to obtain a source flux from coastal BW, we will also employ the scale factor, k , discussed above to link the size distributions and concentrations measured during SEAS to the beach gradient. This gradient is established by the flux from the observed BW bubble coverage. Subsequent generalization of this BW flux to oceanic conditions also requires that we assume that it can be scaled appropriately through an empirical expression such as that derived by *Monahan et al.* [1986] relating whitecap coverage to wind speed.

[29] As the bubble field evolves it continually produces particles at the surface that mix aloft. SSA are generated from bubbles that rise to the ocean surface and burst both in front of and behind a BW. At BAFS, the initial breaking point for a wave was typically measured to be (L) 35 m from the shoreline (Figure 2) and took 22 s to reach the beach indicating a mean wave speed of 1.6 m/s. Digital imagery of incoming BWs taken from the tower and from the beach were used to estimate typical bubble coverage of the wave front and the area behind the advancing wave front (Figure 2). The initial width of the wave front, w_o (defined as 100% visual bubble coverage), was estimated at 2 ± 0.5 m immediately after the break. During the advance to shore this wave front appeared to diminish in width linearly with time but rarely completely dissipated. Consequently we use a mean width of $0.5 w_o$ over the 35 m to shore.

[30] Behind the wave front is an irregular, but extended area of rising bubbles. As the front progressed to shore this area between the front and its initial break point increases even though the fraction of that area covered by bubbles

gradually decreases. Numerous visual examinations of BW images indicated that the mean percentage occupied by bubbles (A_{avg}) behind the wave front over the total distance traveled by a BW was $\sim 40\%$ ($\pm \sim 12\%$). On the basis of these observations, and ignoring second-order corrections to L for the wave front, the mean BW bubble coverage can be expressed as $[(A_{avg} * L) + (0.5w_o)] dl$, where dl is an element of length along the BW front. The total number flux from the bubble surface is a product of the effective flux for 100% bubble coverage, S_{100} , and the mean BW bubble coverage.

[31] For suitably long averaging times, the horizontally advected aerosol flux equals the effective production flux over the surf zone plus the background aerosol flux. Because we have already removed the background flux in our definition of C_s , then we are only concerned here with the SSA production flux. The profile measured at a point on the beach with a top at height, h , reflects the net effect of SSA production and mixing during advection to that point. This profile, advected with the mean wind, yields the horizontal flux over time τ and width dl at the beach location where plume height was established as $4 \text{ m} \pm 0.6 \text{ m}$. We can use the same dl for this flux because on average the wind was essentially orthogonal to the waves at this site. We previously demonstrated that this mean profile concentration can be represented by multiplying our measured 5 m tower C_s concentration by the scale factor, k . Hence, for the typical wind speed, V_{wind} , we can set this advective flux equal to the source flux using equation (1). This relates a “steady state” mean C_s (as measured at 5 m on tower) for coastal BW plumes to the mean bubble coverage. Both represent averages over the kind of data shown in Figure 3.

$$S_{100} [A_{avg}L + 0.5w_o] \tau dl = C_s k (V_{wind}) h \tau dl \quad (1)$$

[32] This yields equation (2) as the SSA source flux for 100% bubble coverage, S_{100} .

$$S_{100} = \frac{C_s \cdot k \cdot V_{wind} \cdot h}{A_{avg} \cdot L + 0.5w_o} \quad (2)$$

where variables and their uncertainties are estimated as

C_s	measured mean BW CNhot (background removed) at 5 m, $30 \pm 5.3 \text{ cm}^{-3}$;
k	multiplier for tower C_s compared to mean profile, 1.5 ± 0.3 ;
V_{wind}	mean surf zone wind speed, $7.3 \pm 1.1 \text{ m/s}$;
h	height of plume layer for beach profile, $4 \pm 0.6 \text{ m}$;
A_{avg}	mean bubble fractional coverage area between waves, 0.4 ± 0.12 ;
L	distance wave travels to shore, $35 \text{ m} \pm 3 \text{ m}$;
w_o	initial width of BW bubble front, $2 \pm 0.5 \text{ m}$.

[33] The product of measured C_s and V_{wind} should be constant for a constant bubble fraction. A constant mean surface bubble coverage (source term) implies the mean measured concentration will decrease (increase) inversely with an increasing (decreasing) wind via a dilution effect [*Clarke and Kapustin, 2003*]. This dependency can be used to explore the consistency of this approach. However, in

Table 1. Coefficients for A_i in Equation (3) Describing S_{100} Over Three D_p Intervals

Coefficient	D_p Range, ^a μm		
	0.01–0.132	0.132–1.2	1.2–8.0
β_0	-5.001E^3	3.854E^3	4.498E^2
β_1	0.808E^6	1.168E^4	0.839E^3
β_2	-1.980E^7	-6.572E^4	-5.394E^2
β_3	2.188E^8	1.003E^5	1.218E^2
β_4	-1.144E^9	-6.407E^4	-1.213E^1
β_5	2.290E^9	1.493E^4	4.514E^{-1}

^aRead -5.001E^3 as -5.001×10^3 .

general, significantly higher V_{wind} could also lead to larger approaching open ocean waves that should lead to larger surf, an earlier wave break and possibly an increased bubble coverage fraction as well as changes in vertical mixing, etc. Even so, we are only interested in establishing the relation of observed C_s to observed bubble coverage for our measurements period and for these relatively stable conditions.

[34] In order to establish C_s for these stable BW conditions we use data from SEAS for JD 114 to JD 117.3 [Clarke and Kapustin, 2003]. C_s is the differences in CNhot at 5 m (impacted by BW) and CNhot at 20 m (background values) [see Clarke et al., 2003, Figure 2]. These data exhibited the above mentioned inverse dependency between C_s and wind speed. For the typical wind speed in this period of 7.3 ms^{-1} we obtained a C_s value of 30 cm^{-3} with $\text{SD} = \pm 5.3$. This yields an integral number flux for 100% bubble coverage, S_{100} , of $\sim 8.8 \times 10^3 \text{ cm}^{-2} \text{ s}^{-1}$.

[35] Uncertainties in V_{wind} were calculated as the standard deviation of the measured quantity while L and w_o were estimated from physical measurements in the surf zone. Of course, a different turbulent structure and profile might be expected under winds significantly different from those experienced here. The profile at this location could change accordingly and would have to be measured but the flux per unit bubble coverage is assumed not to change. The uncertainty for A_{avg} was estimated from the variations in bubbles from BWs captured by multiple digital images. The resulting overall uncertainty of 45% in S_{100} was calculated from the uncertainties of the terms in equation (2) summed in quadrature. We recognize this flux may be sensitive to other meteorological and environmental factors that influence production. Some of these include sea surface temperature, salinity [Lewis and Schwartz, 2004] and surfactant concentration. However, the possible effects of these influences are not well understood [Lewis and Schwartz, 2004] and therefore will not be included here.

3.4. Parameterization and Scaling

[36] The integral number flux (S_{100}) can be used to scale the normalized mean BW refractory size distribution previously established during SEAS (Figure 1) to yield our size resolved source function for 100% bubble coverage. Agreement with independent measurements of total number (dominated by small D_p) and between measured and calculated σ_{sp} (dominated by large D_p) during SEAS [Clarke et

al., 2003] implies an overall uncertainty in fitting this distribution of $\sim 10\%$. Allowing for this size distribution fitting uncertainty increases the overall uncertainty in the S_{100} flux distribution to $\sim 50\%$. The SSA distribution was fit here with three fifth-order polynomial regressions of the form

$$A_i = \beta_0 + \beta_1 D_p + \beta_2 D_p^2 + \beta_3 D_p^3 + \beta_4 D_p^4 + \beta_5 D_p^5 \quad (3)$$

for the three D_p intervals given in Table 1. The indicated coefficients preserve the shape of the distribution to within 1%. The mean number flux (F_N) per log D_p interval is calculated by summation of equation (3) for each D_p range.

$$\left(\frac{dF_N}{d \log D_p} \right)_{BW} = \sum_{i=1}^3 A_i \quad (4)$$

[37] As mentioned earlier, we assume here that a unit of surface bubble coverage results in the same SSA flux for both coastal and open ocean environments for low to moderate wind speeds. We do not consider high winds where wave tearing and spume production are active. Hence we assume that equation (4) can be applied to oceanic conditions by multiplying it by the fractional whitecap coverage, W . An empirical expression derived by Monahan et al. [1986] describes whitecap coverage as a function of wind speed where U_{10} is the wind speed at a height of 10 m.

$$W = (3.84\text{E}^{-6})(U_{10}^{3.41}) \quad (5)$$

[38] Although alternate formulations are possible we will use this relationship to describe the oceanic mean size-resolved number flux from whitecaps as a function of wind speed. This flux expression is applicable over $0.01 \leq D_p \leq 8 \mu\text{m}$ with the above estimated uncertainty of 50% and it can be converted to surface area, volume and mass fluxes by multiplying the appropriate factors and integrating over size.

3.5. Comparison With Currently Used Source Functions

[39] Here we provide comparisons of our SSA source function with other commonly referenced approaches. The first involves laboratory simulated bubble generation mechanisms scaled with observations of oceanic whitecap coverage as a function of wind speed [Monahan et al., 1986] (M86) and [Martensson et al., 2003] (MN03). The second utilizes field observations to derive production rates leading to the measured concentration from a fixed height [de Leeuw et al., 2000]. Our derived number flux and these prior estimates are presented in Figure 6 over their reported applicable size range. Because these functions were reported in different formats we present them here graphically as dry diameter, D_p . The radius at formation (r_o) is approximately twice radius at RH = 80% (r_{80}). The value of r_{80} is also about twice the dry radius such that physical dimensions exhibit the following equivalence ($0.5r_o \approx r_{80} \approx D_p$). All fluxes have been scaled to oceanic conditions corresponding to $U_{10} = 9 \text{ m/s}$ following equation (4) and have been expressed as $dF_N/d \log D_p \text{ (cm}^{-2} \text{ s}^{-1})$ in order to

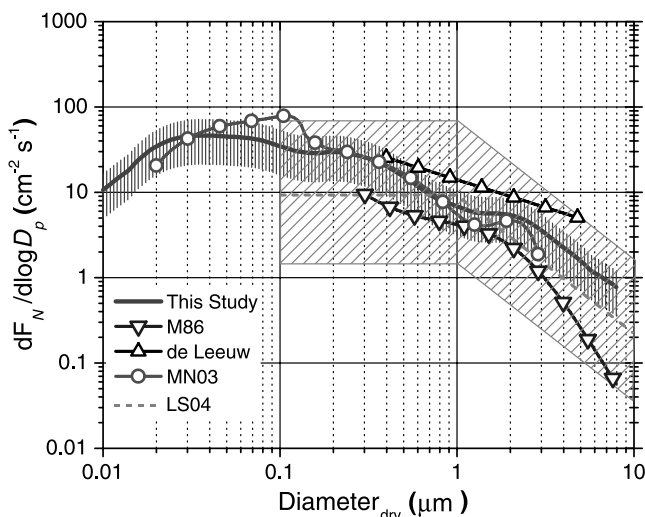


Figure 6. Derived source function compared to others available in literature, as discussed in text. All flux estimates have been scaled to oceanic conditions under $U_{10} = 9$ m/s and converted to dry diameters.

facilitate comparison with size resolved fluxes estimated elsewhere [Martensson *et al.*, 2003].

[40] In particular, our derived coastal source flux also compares very well to the laboratory study of MN03 at 25°C over most of the range. Their data were generated from bubble chamber simulations with dissolved synthetic sea salt in pure Milli-Q water, similar to typical environmental conditions (salinity, water temperature) we experienced at BAFS. Although MN03 deviates slightly for D_p near 0.1 μm , similarities with our natural ocean BW flux, including ultrafine sizes, suggests that production mechanisms are representative of coastal BWs. Other source functions are limited to larger particle diameters and our flux is slightly lower than the *de Leeuw et al.* [2000] data over the applicable range $0.4 \leq D_p \leq 5$ μm . This was collected on the coast of California using optical particle counters under similar conditions to that of the present study. On the other hand, our derived flux is somewhat larger than M86.

[41] We also note that recent results for a wind speed 8 ms^{-1} based upon the “concentration build up” method [Reid *et al.*, 2001] were shown to be ~ 30 –50% higher than the M86 values at 8 ms^{-1} for sizes between 1 and 10 μm and even greater at smaller sizes. This very different approach involved aircraft measurements of the concentration increase of sea salt during offshore flow over 35 km for various wind speeds. When corrected to the 9 ms^{-1} used in Figure 6, the Reid *et al.* data (not shown for clarity) at smaller sizes fall well within the uncertainty range indicated for our flux while their flux for the larger sizes lies at the lower limit of our range.

[42] The heavy dashed line labeled LS04 represents the mean of 10 published data sets based upon the “whitecap method” for a wind speed of 10 ms^{-1} , as presented and discussed by *Lewis and Schwartz* [2004] only rescaled here with equation (5) to a 9 ms^{-1} wind speed for consistency with the other data shown. The LS04 sets were argued to lie within variability of a factor of 7 [Lewis and Schwartz, 2004], as indicated here. We have not included the possible

uncertainty in W , also discussed by these authors, because the same equation (5) was used for all data sets in Figure 6. Note that for most size ranges, our source function (with its estimated uncertainty factor of ~ 1.5) lies within about a factor of 2 of (a) the representative expression for the “whitecap method”; (b) the *de Leeuw et al.* [2000] data; (c) the M86 values and (d) the aforementioned [Reid *et al.*, 2001] data (not shown). While this consistency does not confirm the validity of our source function at this level of confidence it does indicate that it is consistent with these recent studies at the larger size range and that it is a reasonable functional form to use. This extends the oceanic SSA source function over sizes from 0.01 μm to ~ 10 μm . We also feel that for sizes below 2 μm that dominate the number and CCN flux (Figure 1) these diverse approaches (including the Reid *et al.* [2001] “concentration build up method”) are within about a factor of 2, suggesting the factor of 7 uncertainty estimated for LS04 possibly overstates current uncertainties in the “whitecap method.”

4. MBL Aerosol: Sea Salt, Sulfate, and CCN

[43] We assume here that our source flux can be applied to open ocean production but we also recognize that many other factors that remain poorly understood may influence this dependency. Some concerns are: whether the bubbles producing SSA subsequent to the visible phase of the whitecap continue to scale with the whitecap area; how to define the whitecap area; whether all whitecap areas are equally productive; size dependencies in whitecap lifetimes and related issues discussed at length elsewhere [Lewis and Schwartz, 2004]. Even so, a limited time sequence of images for the data discussed here did reveal direct links between observable whitecap coverage and fluctuations in SSA concentrations (not shown). Hence below we will estimate oceanic SSA fluxes by multiplying our S_{100} source function by the percentage of oceanic white cap coverage.

4.1. MBL Aerosol From the Free Troposphere

[44] Even in MBL regions free of pollution and continental aerosol influence, as discussed here, SSA is not the only natural aerosol flux into the marine boundary layer. As we mention in the introduction, the FT can be a dominant source of volatile sulfate aerosol into the MBL in clean marine regions. These appear to originate in regions of cloud outflow aloft and then increase in size during aging and subsidence [Clarke *et al.*, 1998]. The number peak dry diameter of this mode has been found to lie between 0.03 and 0.05 μm near Tasmania [Clarke *et al.*, 1996, Figure 7], between 0.05 and 0.06 μm over Hawaii [Clarke *et al.*, 1996, Figure 4], between about 0.04 and 0.08 μm over the North Pacific near Oregon [Hoppel *et al.*, 1994, Figure 8], near 0.06 μm over CI [Clarke *et al.*, 1998, Figure 12], and between 0.07 and 0.09 μm on subsequent CI flights [Clarke and Kapustin, 2002, Figure 11]. This mode diameter depends upon time since nucleation, available precursor concentrations, aerosol surface area, etc., but it appears to be a persistent mode that can be entrained into the MBL and provide a volatile natural non-SSA component to the MBL aerosol. Concurrent aerosol size and chemical measurements in the tropics [Clarke *et al.*, 1998] suggested that the FT aerosol is primarily sulfate, although other species

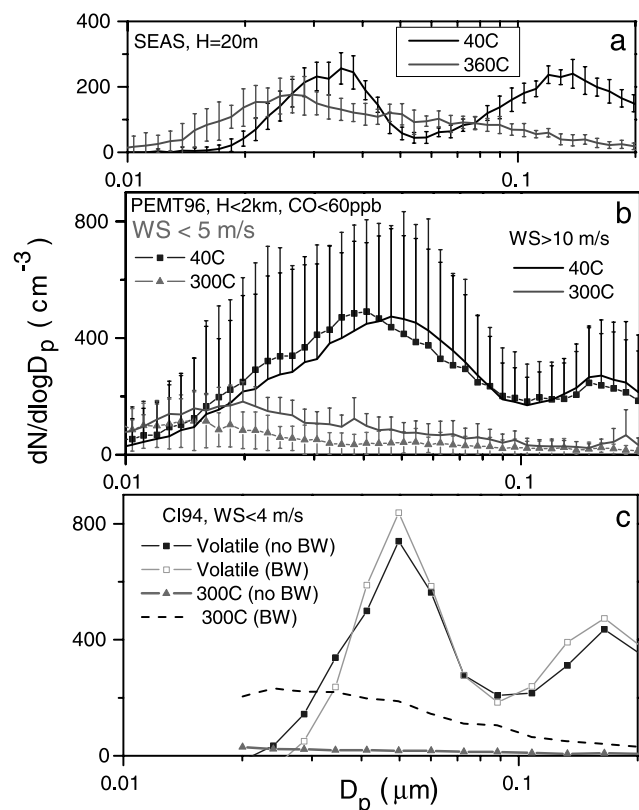


Figure 7. (a) Open ocean DMA distributions (and standard deviations) from SEAS get smaller upon heating with little change in number, but only 10% of volume remains (not shown), indicating internally mixed volatile and refractory components. (b) PEM-T distributions (in tropics below 2 km) for winds below 5 m s^{-1} and for winds above 10 m s^{-1} . Bars indicate 1 standard deviation for data in Figure 7b, but only positive deviations are shown for unheated distributions in order to maintain figure clarity. (c) CI refractory and volatile distributions for onshore flow showing few refractory aerosols. A large increase in refractory concentrations (dashed line) occurs when coastal breaking waves reached tower while volatile distributions remain unchanged.

such as organics appear possible elsewhere [Van Dingenen *et al.*, 1999; Zhou *et al.*, 2001]. For the purpose of this paper a sulfate aerosol will be assumed. Similar monomodal distributions of sulfate that include sizes effective as CCN have also been predicted globally in the FT above the inversion [Adams and Seinfeld, 2002].

[45] We note that this FT flux differs in several ways from a sea-salt flux. The latter represents newly formed particles injected directly into the MBL air through its lower surface. Consequently, in the absence of removal, MBL concentrations of SSA could increase indefinitely for a persistent SSA flux. However, the FT aerosol are introduced along with the FT air into the MBL and the number mixing ratio of the FT aerosol present in the MBL cannot exceed that in the entrained FT air regardless of the strength or persistence of the entrainment.

[46] The nature of this entrainment process also needs to be considered. The top of the MBL is typically defined in terms

of a temperature inversion that separates the generally well-mixed MBL from the more stably stratified FT. The latter is often associated with large-scale subsidence (e.g., Pacific high-pressure system) that feeds the FT aerosol toward a subsidence inversion above the MBL [Clarke *et al.*, 1996]. Exchanges of air across the inversion involve not only the transport of aerosol but also of air with different temperatures, humidity gas phase concentrations, etc. Over most of the ocean between say 45N to 45S this exchange is driven by turbulent motions penetrating upward from the MBL that can “engulf” FT air into the MBL which is deepened as a result [Garratt, 1994]. This process reflects a combination of dynamic and thermodynamic effects that tend to maintain a sharp temperature inversion and move it upward. Hence this mixing “through” the inversion can be visualized as a unidirectional entrainment relative to the inversion that effectively deepens the boundary layer [Stevens *et al.*, 2003]. Such boundary layer growth is common in subtropical air advected toward the ITCZ but has been observed and modeled in other regions [Jiang *et al.*, 2001] using large eddy simulations. Divergence in the MBL can also act to reduce the growth in boundary layer height otherwise associated with entrainment. This divergence is frequently associated with motion toward organized deep convection. Such convection (e.g., squall lines, ITCZ) vents air into the FT and often scavenges aerosol mass and CCN through precipitation. This precipitation is the primary sink of MBL CN and CCN but removal generally takes place over smaller scales and locations than the larger-scale entrainment discussed here.

[47] The effect of boundary layer growth through entrainment is significant. For example, an MBL with an inversion at 800 m and a typical entrainment rate of say 0.5 cm s^{-1} will double in height in two days (assuming no MBL divergence). Assuming no active removal terms over this time, this influx of FT air would also dilute any preexisting MBL aerosol concentrations by a factor of 2. It would also reduce any concentrations of SSA generated during these two days by a factor of 2 compared to concentrations that would have resulted had entrainment of FT air not occurred. The ratio of the concentration increase of the FT to the SSA aerosol introduced over these two days would correspond to the ratio of the fluxes. However, when preexisting background aerosol, advection, physiochemical evolution and size-dependent removal terms are included then the relation between actual MBL concentrations and these fluxes becomes complex and requires inclusion of all relevant terms [Pierce and Adams, 2006].

[48] The refractory sea-salt and volatile sulphate aerosol can mix, age and participate in nonprecipitating MBL cloud processes for days before being removed, commonly by precipitation. Such ageing and cycling can add mass to SSA through heterogeneous processes. Figure 7a shows examples of unheated DMA distributions observed in Hawaii during SEAS for onshore flow at 20 m not influenced by coastal BW. The minimum near $0.06 \mu\text{m}$ arises when larger sizes activate to become cloud droplets for a given cloud supersaturation allowing them to rapidly add mass through in-cloud processes [Hoppel *et al.*, 1994]. Particles too small to activate grow less and the modes separate as a result of cloud passages.

[49] Our measurements are consistent with this process. Upon heating, the residual refractory mode of the SEAS

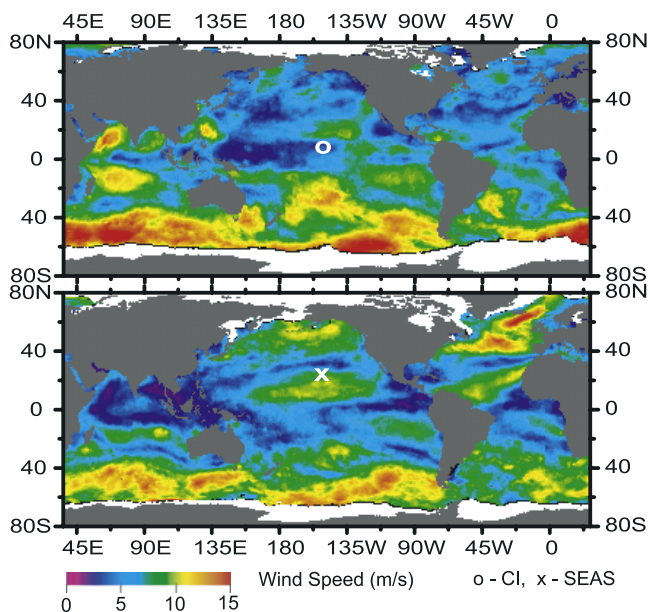


Figure 8. Weekly average global scatterometer winds (ERS-AM1 microwave radiometer, <http://www.ifremer.fr/cersat>) for the CI (circle) measurement period (1994) and SEAS (cross) period (2000). Regional average scatterometer winds upwind of CI are $\sim 3\text{--}5\text{ m s}^{-1}$ and, for SEAS, $\sim 7\text{--}9\text{ m s}^{-1}$.

open ocean aerosol (Figure 7a) is clearly reduced to much smaller sizes. However, the total number (area under plot) changes less than 30% upon heating, in spite of 90% of the submicrometer mass being volatile. This implies $\sim 70\%$ of these particles were internal mixtures of volatile and refractory aerosol. This residual refractory distribution in aged marine aerosol (Figure 7a) is similar to that from BW (Figure 1). This behaviour is consistent with the accumulation of volatile mass upon the refractory SSA aerosol [Murphy et al., 1998; Sievering et al., 2004; Zhou et al., 2001]. This refractory SSA component may help account for the stability of mode sizes often observed in marine aerosol [Heintzenberg et al., 2004].

[50] Similar refractory distributions are present in remote oceanic aerosol (Figure 7b) collected below 2 km during NASA Pacific Exploratory Missions–Tropics (PEM-T) flown in 1996 between Hawaii and Easter Island. Most data are from the South Pacific, where MBL winds were commonly 5 to 10 m s^{-1} . Here we only show distributions for winds below 5 m s^{-1} ($n = 52$) or above 10 m s^{-1} ($n = 41$). The unheated average number distributions are very similar in magnitude and variability but average refractory SSA concentrations are twice as high for the higher wind speeds, consistent with enhanced SSA production. These refractory distributions are also similar to SEAS (Figure 7a) although volatile number fractions are much higher. These higher volatile concentrations may reflect higher entrainment rates and/or weaker removal by precipitation [Clarke et al., 1996; Van Dingenen et al., 1999].

[51] We also note that unheated distributions for higher wind speeds have diameters $\sim 10\text{--}20\%$ larger than the low-wind-speed cases. This corresponds to submicrometer volatile volumes that are $\sim 50\%$ larger under higher winds. This

would be consistent with a natural sulfate component linked to DMS oxidation in the MBL [Clarke and Porter, 1993] that is expected to increase because of an enhanced gas transfer coefficient. The latter is expected to increase about a factor of 3 because of increased bubble coverage associated with a mean wind increase from about 5 to 10 m s^{-1} [Monahan and Torgersen, 1990].

4.2. Christmas Island, Low Winds, and FT Entrainment

[52] It is revealing to compare the distributions in Hawaii and the South Pacific (Figures 7a and 7b) to those for CI (Figure 7c) where winds were consistently low in steady easterly equatorial flow. Mean satellite derived winds were $\sim 2\text{--}5\text{ m s}^{-1}$ near CI (circle) compared to $6\text{--}9\text{ m s}^{-1}$ during SEAS (cross) (Figure 8), consistent with whitecaps being rare at CI but common during SEAS. Figure 7c shows heated and unheated open ocean distributions at CI during a 30 hr period on DOY 220–222 with a measured tower mean wind of 4.8 m s^{-1} ($\text{SD} = 1.8\text{ m s}^{-1}$), mean coastal wind often exceeds open ocean values because of influence from island surface heating and localized convection). CI shows far less refractory aerosol than SEAS or PEM-T, as can be expected since CI winds are usually below the limit for generation of whitecaps. A similarly large volatile fraction was also reported for 28 measurements over two days in the South Pacific near 15S [Hoppel and Frick, 1990].

[53] Occasionally, winds at CI veered south and mixed aerosol from coastal BWs (breaking $\sim 200\text{--}400\text{ m}$ down the coast) up to the top of the tower. This resulted in no change in the volatile component but a marked increase in refractory aerosol (Figure 7c) with a distribution similar to coastal BW during SEAS (Figure 1) [Clarke et al., 2003]. Hence BW at both island locations produce refractory particle distributions extending down below $0.02\text{ }\mu\text{m}$. The volatile number at CI are dominated by aerosol entrained into the MBL from the free troposphere, FT [Clarke et al., 1996], with a peak often near $0.08\text{ }\mu\text{m}$ [Clarke and Kapustin, 2002]. However, repeated processing through MBL clouds and growth through gas to particle conversion is associated with active sulfur photochemistry in this region [Bandy et al., 1996]. This can add mass to activated sizes and can separate cloud activated from the unactivated interstitial sizes to yield a minimum (Figure 7c) in the vicinity of $0.08\text{ }\mu\text{m}$ [Clarke et al., 1996; Hoppel and Frick, 1990; Hoppel et al., 1994].

4.3. Relative Role of SSA and FT Aerosol Fluxes on MBL CCN

[54] The observations above indicate that the remote MBL aerosol is maintained by a surface flux of refractory SSA and an entrainment flux of aerosol from the FT. These may persist as separate modes over many days as coagulation between these sizes should be slow [Van Dingenen et al., 1999]. Regional differences in wind speeds (e.g., Figure 8) and the exponential dependence of whitecap coverage on wind speed imply that the SSA contribution will be highly variable. Figure 9 shows the SSA production flux for winds of 5 , 10 , 15 m s^{-1} using our S_{100} flux scaled with estimated whitecap coverage approximated by equation (5). By comparison, typical

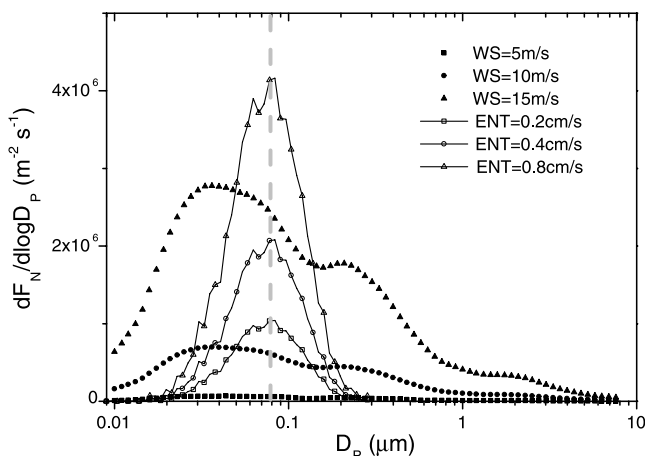


Figure 9. Estimated surface flux distributions for SSA (solid symbols) based upon our SEAS size distributions and scaled to wind speeds of 5, 10, and 15 ms^{-1} [Monahan *et al.*, 1986], and nominal fluxes through the top of the MBL for CI example sulfate aerosol (open symbols) entrained at 0.2, 0.4, and 0.8 cm s^{-1} .

unpolluted FT particle concentrations above the MBL inversion are $\sim 300 \pm 100 \text{ cm}^{-3}$ [Clarke and Kapustin, 2002]. When multiplied by low to moderate entrainment rates of 0.2, 0.4 and 0.8 cm s^{-1} , these yield the nominal size resolved FT fluxes into the MBL also shown in Figure 9. The entrainment rate for tropical CI was $\sim 0.6 \pm 0.2 \text{ cm s}^{-1}$ [Clarke *et al.*, 1996] and suggest a number flux into the MBL from the FT of $\sim 180 \pm 80 \text{ cm}^{-2} \text{ s}^{-1}$.

[55] This characterization of SSA fluxes from the surface and an FT aerosol flux through the inversion provides a framework for understanding the variability in MBL aerosol number. Fluxes of nominal CCN into the MBL from both SSA and FT sources can also be estimated from sizes larger than $0.08 \mu\text{m}$ (Figure 9) since both contribute effective CCN above this size. About half of both FT and SSA particles can have dry diameters larger than $\sim 0.08 \mu\text{m}$ indicating that both sources can introduce about half of their flux at sizes already effective as CCN, even though SSA activate at somewhat smaller sizes for the same supersaturation. The total CCN flux is clearly dominated by SSA in regions of higher winds with weak entrainment while in regions of persistent low wind, like CI, the FT source dominates.

[56] Table 2 illustrates the relative contribution of SSA to the total flux of nominal CCN into the MBL for various wind speeds and entrainment rates. Here we assume for comparison that $\sim 50\%$ of the SSA flux and $\sim 40\%$ of the FT flux are in CCN sizes larger than $0.80 \mu\text{m}$. The range of values for the SSA flux reflects the uncertainty in the S_{100} flux of 50% for a fixed entrainment distribution (Figure 9). The influences of continental aerosol sources, different FT distributions, various removal fluxes, aerosol growth, possible coupling between mean wind speeds and entrainment rates are not considered here. Consequently, actual variability is expected to be larger. Nevertheless, the SSA flux contribution varies from insignificant (5%) to dominant (over 90%). About 20–50% of the CCN flux into the MBL is estimated to be SSA at common intermediate wind speeds and entrainment rates.

[57] As mentioned earlier, these fluxes cannot be compared directly to MBL concentrations because of issues of prior history, lifetimes, removal, aging, etc. Even so, these values are consistent with the low percentage of refractory CCN (less than 10%) observed for low winds and the moderate entrainment observed at CI. Flux ratios are also similar to concentration ratios for intermediate entrainment and moderate winds ($7 \pm 2 \text{ m s}^{-1}$) during SEAS where a refractory fraction near 60% was common. About 70% of the ocean surface lies between 40°N and 40°S under an inversion that grows toward the equator as a result of entrainment. The surface winds are typically between 5 and 10 ms^{-1} and Table 2 suggests that SSA may contribute between 20 and 65% of the direct CCN flux into the MBL over these regions. A SSA CCN flux greater than 75% appears likely at higher latitudes characterized by higher winds [O’Dowd and Smith, 1993]. However, in most cases high winds are episodic with the exception of regions like the Southern Ocean (Figure 8).

5. Discussion and Conclusions

[58] Measurements during SEAS and those of 2004 established coastal BW refractory aerosol size distributions from $0.01 \leq D_p \leq 8 \mu\text{m}$ for coastal BW sea-salt production. This distribution was combined here with assessments of near-surface concentrations associated with the observed bubble coverage from BWs to derive a source function for the size resolved number flux per unit of bubble covered surface. When scaled to oceanic conditions, this source flux was shown to be consistent with several previously published estimates. However, our new source function extends SSA aerosol production down to $0.01 \mu\text{m}$, an order of magnitude smaller than previously characterized for oceanic BWs.

[59] This and our simplified flux estimate from the FT assume the MBL and FT are neither impacted by nor interacting with emissions of continental and pollution aerosol. Actual MBL CCN and SSA concentrations also depend upon complex aerosol dynamics and size-dependent growth and removal terms [O’Dowd *et al.*, 1999; Van Dingenen *et al.*, 1999; Yoon and Brimblecombe, 2002]. Moreover, a surface source of DMS can lead to sulfate production and heterogeneous growth of SSA and FT aerosol that transforms externally mixed aerosol into internal mixtures [Murphy *et al.*, 1998; Sievering *et al.*, 1999; Zhou *et al.*, 2001]. This is consistent with observed open ocean aerosol volatility discussed for Figures 7a and 7b. Particles activated as CCN [Hoppel *et al.*, 1994] increase their mass as a result of enhanced heterogeneous chemistry and condensation possible upon the large cloud droplet

Table 2. Estimated Percent of CCN ($D_p > 0.08 \mu\text{m}$) Flux Into the MBL as SSA at Indicated Wind Speeds and Entrainment Rates of Example FT Aerosol^a

Entrainment	Wind Speed		
	5 ms^{-1} (3–6)	10 ms^{-1} (25–64)	15 ms^{-1} (100–240)
0.2 cm s^{-1} (24)	11–21%	52–75%	81–91%
0.4 cm s^{-1} (48)	6–12%	35–58%	68–84%
0.8 cm s^{-1} (96)	3–6%	21–40%	52–72%

^aParentheses show associated particle number flux ($\# \text{ cm}^{-2} \text{ s}^{-1}$).

surface area. However, their larger size also increases the likelihood of subsequent removal through precipitation. Hence more complex and dynamic interaction models are needed to translate these estimated fluxes into resulting size-resolved MBL concentrations. Recent application of our ultrafine SSA flux parameterization to such a model (GISS II–prime GCM) that includes interactive sulphur chemistry has revealed regions where the addition of sea salt increases model CCN (0.2% saturation) by 150% to 500% compared to that of sulphate aerosol alone [Pierce and Adams, 2006]. They also found that the presence of the SSA ultrafine component ($D_p < 0.1 \mu\text{m}$) alone increased the MBL CCN by 50% relative to runs without the ultrafine sea salt primarily because of their growth up to CCN sizes via condensed sulphate.

[60] These observations also impact the so called CLAW hypothesis [Charlson *et al.*, 1987] that suggests increased production of dimethyl sulfide, DMS, could result in a proportionally greater nucleation in the MBL leading to proportionally increased CCN and enhanced cloud albedo. Recent studies have brought CLAW into question as MBL nucleation appears uncommon both as measured [Clarke *et al.*, 1996] and as modeled [Katoshevski *et al.*, 1999]. Here we demonstrated that CCN can originate directly from both the ocean surface and the FT. While the FT sulfate flux may be linked to surface DMS, the process is more complex than envisioned in the CLAW hypothesis and only a small fraction of the DMS flux participates directly in their formation. However, the fraction of DMS exported from the MBL in deep convective clouds can result in nucleation aloft near cloud outflow [Clarke *et al.*, 1998]. After aging and subsidence these can be entrained into the MBL. The particle flux from the FT into the lowest 1000 m are often near 50 particles $\text{cm}^{-2} \text{s}^{-1}$ (Table 2) and equivalent to concentration increases of $\sim 80 \text{cm}^{-3} \text{day}^{-1}$. For a 2–4 day residence time, these fluxes can also account for typical CN concentrations of several hundred per cm^3 commonly observed over these regions [Clarke *et al.*, 1996; Clarke and Porter, 1993].

[61] Both SSA and FT sources include a reservoir of nuclei smaller than $0.08 \mu\text{m}$ that can become effective as CCN through heterogeneous growth. If precursors, such as DMS, remain constant then growth of smaller particles to CCN sizes will be most rapid when precipitation reduces the number of larger CCN and the corresponding uptake onto their larger surface area. This will enhance the growth rate of smaller sizes up to CCN sizes and replenish those lost through precipitation. This process could thereby buffer MBL CCN concentrations against depletion and reduce variability. The loss of volatile coatings upon heating suggests that this growth can occur on SSA sizes as small as 10 nm, as was also evident in the previously mentioned model results [Pierce and Adams, 2006]. Similar observations have been made for sizes down to 60 nm [Murphy *et al.*, 1998] and larger [Sievering *et al.*, 2004]. Hence the major link between the DMS flux, MBL sulfate and CCN will be through an increase in existing particle size rather than number. This implies a weaker influence upon cloud albedo arising from changes in DMS emissions than suggested by CLAW. The influence of these sources of CCN from SSA or FT aerosol and the evolution of smaller diameters

below $0.08 \mu\text{m}$ will need to be included in models of marine aerosol evolution and CCN.

[62] **Acknowledgments.** We thank the Office of Naval Research for their support under N00014-94-1-0539 and N00014-96-1-0320 (mod. A00007) and NASA (NCC-1-315), which made these measurements possible. We also appreciate use of the ERS-AM1 microwave radiometer from <http://www.ifremer.fr/cersat>. This is University of Hawaii SOEST contribution 6697.

References

- Adams, P. J., and J. H. Seinfeld (2002), Predicting global aerosol size distributions in general circulation models, *J. Geophys. Res.*, *107*(D19), 4370, doi:10.1029/2001JD001010.
- Allan, J. D., et al. (2004), Submicron aerosol composition at Trinidad Head, California, during ITCT 2K2: Its relationship with gas phase volatile organic carbon and assessment of instrument performance, *J. Geophys. Res.*, *109*, D23S24, doi:10.1029/2003JD004208.
- Andreas, E. L. (1998), A new sea spray generation function for wind speeds up to 32m s^{-1} , *J. Phys. Oceanogr.*, *28*(11), 2175–2184.
- Bandy, A., D. C. Thornton, B. W. Blomquist, S. Chen, T. P. Wade, J. C. Ianni, G. M. Mitchell, and W. Nadler (1996), Chemistry of dimethyl sulfide in the equatorial Pacific atmosphere, *Geophys. Res. Lett.*, *23*(7), 741–744.
- Blanchard, D. C., and A. H. Woodcock (1957), Bubble formation and modification in the sea and its meteorological significance, *Tellus*, *9*, 145–158.
- Campuzano-Jost, P., C. D. Clark, H. Maring, D. S. Covert, S. Howell, V. Kapustin, K. A. Clarke, E. S. Saltzman, and A. J. Hynes (2003), Near-real-time measurement of sea-salt aerosol during the SEAS campaign: Comparison of emission-based sodium detection with an aerosol volatility technique, *J. Atmos. Oceanic Technol.*, *20*(10), 1421–1430.
- Campuzano-Jost, P., D. Donohoue, and M. H. B. Hynes (2004), Submicron sea salt aerosol inside and outside of the surf plume: Size segregated and total sea salt aerosol distributions by single particle analysis at a coastal marine site, *Eos Trans. AGU*, *84*(47), Fall Meet. Suppl., Abstract A31C-0082.
- Charlson, R. J., J. E. Lovelock, M. O. Andreae, and S. G. Warren (1987), Oceanic phytoplankton, atmospheric sulfur, cloud albedo and climate, *Nature*, *326*(6114), 655–661.
- Cipriano, R. J., E. C. Monahan, P. A. Bowyer, and D. K. Woolf (1987), Marine condensation nucleus generation inferred from whitecap simulation tank results, *J. Geophys. Res.*, *92*(C6), 6569–6576.
- Clarke, A. D. (1991), A thermo optic technique for in-situ analysis of size-resolved aerosol physicochemistry, *Atmos. Environ., Part A*, *25*(3–4), 635–644.
- Clarke, A. D., and V. N. Kapustin (2002), A Pacific aerosol survey. Part I: A decade of data on particle production, transport, evolution, and mixing in the troposphere, *J. Atmos. Sci.*, *59*(3), 363–382.
- Clarke, A. D., and V. N. Kapustin (2003), The Shoreline Environment Aerosol Study (SEAS): A context for marine aerosol measurements influenced by a coastal environment and long-range transport, *J. Atmos. Oceanic Technol.*, *20*(10), 1351–1361.
- Clarke, A. D., and J. N. Porter (1993), Pacific marine aerosol: 2. Equatorial gradients in chlorophyll, ammonium, and excess sulfate during Saga-3, *J. Geophys. Res.*, *98*(D9), 16,997–17,010.
- Clarke, A. D., Z. Li, and M. Litchy (1996), Aerosol dynamics in the equatorial Pacific Marine boundary layer: Microphysics, diurnal cycles and entrainment, *Geophys. Res. Lett.*, *23*(7), 733–736.
- Clarke, A. D., J. L. Varner, F. Eisele, R. L. Mauldin, D. Tanner, and M. Litchy (1998), Particle production in the remote marine atmosphere: Cloud outflow and subsidence during ACE 1, *J. Geophys. Res.*, *103*(D13), 16,397–16,409.
- Clarke, A. D., F. Eisele, V. N. Kapustin, K. Moore, D. Tanner, L. Mauldin, M. Litchy, B. Lienert, M. A. Carroll, and G. Albercook (1999), Nucleation in the equatorial free troposphere: Favorable environments during PEM-Tropics, *J. Geophys. Res.*, *104*(D5), 5735–5744.
- Clarke, A., V. Kapustin, S. Howell, K. Moore, B. Lienert, S. Masonis, T. Anderson, and D. Covert (2003), Sea-salt size distributions from breaking waves: Implications for marine aerosol production and optical extinction measurements during SEAS, *J. Atmos. Oceanic Technol.*, *20*(10), 1362–1374.
- Deane, G. B., and M. D. Stokes (2002), Scale dependence of bubble creation mechanisms in breaking waves, *Nature*, *418*(6900), 839–844.
- de Leeuw, G., F. P. Neele, M. Hill, M. H. Smith, and E. Vignali (2000), Production of sea spray aerosol in the surf zone, *J. Geophys. Res.*, *105*(D24), 29,397–29,409.

- Dinger, J. E., H. B. Howell, and T. A. Wojciechowski (1970), On the source and composition of cloud nuclei in a subsident air mass over the North Atlantic, *J. Atmos. Sci.*, *27*(5), 791–797.
- Exton, H. J., J. Latham, P. M. Park, S. J. Perry, M. H. Smith, and R. R. Allan (1985), The production and dispersal of marine aerosol, *Q. J. R. Meteorol. Soc.*, *111*(469), 817–837.
- Fuchs, N. A. (1963), On the stationary charge distribution of aerosol particles in a bipolar ionic atmosphere, *Geofis. Pura Appl.*, *56*, 185–193.
- Garratt, J. R. (1994), *The Atmospheric Boundary Layer*, 316 pp., Cambridge Univ. Press, New York.
- Gong, S. L. (2003), A parameterization of sea-salt aerosol source function for sub and super-micron particles, *Global Biogeochem. Cycles*, *17*(4), 1097, doi:10.1029/2003GB002079.
- Heintzenberg, J., W. Birmili, A. Wiedensholer, A. Nowak, and T. Tuch (2004), Structure, variability and persistence of the submicrometre marine aerosol, *Tellus, Ser. B*, *56*(4), 357–367.
- Hoppel, W. A., and G. M. Frick (1990), Submicron aerosol size distributions measured over the tropical and South-Pacific, *Atmos. Environ., Part A*, *24*(3), 645–659.
- Hoppel, W. A., G. M. Frick, J. Fitzgerald, and R. E. Larson (1994), Marine boundary-layer measurements of new particle formation and the effects nonprecipitating clouds have on aerosol-size distribution, *J. Geophys. Res.*, *99*(D7), 14,443–14,459.
- Jiang, H. L., G. Feingold, W. R. Cotton, and P. G. Duynkerke (2001), Large-eddy simulations of entrainment of cloud condensation nuclei into the Arctic boundary layer: May 18, 1998, FIRE/SHEBA case study, *J. Geophys. Res.*, *106*(D14), 15,113–15,122.
- Katoshevski, D., A. Nenes, and J. H. Seinfeld (1999), A study of processes that govern the maintenance of aerosols in the marine boundary layer, *J. Aerosol Sci.*, *30*(4), 503–532.
- Leck, C. A., and E. K. Bigg (1999), Aerosol production over remote marine areas: A new route, *Geophys. Res. Lett.*, *26*(23), 3357–3581.
- Lewis, E. R., and S. E. Schwartz (2004), *Sea Salt Aerosol Production: Mechanisms, Methods, Measurements and Models*, *Geophys. Monogr. Ser.*, vol. 152, 413 pp., AGU, Washington, D. C.
- Martensson, E. M., E. D. Nilsson, G. D. Leeuw, L. H. Cohen, and H. C. Hansson (2003), Laboratory simulations and parameterization of the primary marine aerosol production, *J. Geophys. Res.*, *108*(D9), 4297, doi:10.1029/2002JD002263.
- Monahan, E. C., and T. Torgersen (1990), The enhancement of air-sea gas exchange by oceanic whitecapping, in *Air-Water Mass Transfer*, edited by S. C. Wilhelm and J. S. Gulliver, pp. 608–617, Am. Soc. of Civ. Eng., New York.
- Monahan, E. C., D. E. Spiel, and K. L. Davidson (1986), A model of marine aerosol generation via whitecaps and wave disruption, in *Oceanic Whitecaps and Their Role in Air-Sea Exchange Processes*, edited by E. C. Monahan and G. Mac Niocaill, pp. 167–193, Springer, New York.
- Murphy, D. M., J. R. Anderson, P. K. Quinn, L. M. McInnes, F. J. Brechtel, S. M. Kreidenweis, A. M. Middlebrook, M. Posfai, D. S. Thomson, and P. R. Buseck (1998), Influence of sea-salt on aerosol radiative properties in the Southern Ocean marine boundary layer, *Nature*, *392*(6671), 62–65.
- Nilsson, E. D., U. Rannik, E. Swietlicki, C. Leck, P. P. Aalto, J. Zhou, and M. Norman (2001), Turbulent aerosol fluxes over the Arctic Ocean: 2. Wind-driven sources from the sea, *J. Geophys. Res.*, *106*(D23), 32,139–32,154.
- O'Dowd, C. D., and M. H. Smith (1993), Physicochemical properties of aerosols over the northeast Atlantic: Evidence for wind-speed-related submicron sea-salt aerosol production, *J. Geophys. Res.*, *98*(D1), 1137–1149.
- O'Dowd, C. D., J. A. Lowe, M. H. Smith, and A. D. Kaye (1999), The relative importance of non-sea-salt sulphate and sea-salt aerosol to the marine cloud condensation nuclei population: An improved multi-component aerosol-cloud droplet parametrization, *Q. J. R. Meteorol. Soc.*, *125*(556), 1295–1313.
- Pierce, J. R., and P. J. Adams (2006), Global evaluation of CCN formation by direct emission of sea salt and growth of ultrafine sea salt, *J. Geophys. Res.*, *111*, D06203, doi:10.1029/2005JD006186.
- Porter, J. N., B. R. Lienert, S. K. Sharma, E. Lau, and K. Horton (2003), Vertical and horizontal aerosol scattering fields over Bellows Beach, Oahu, during the SEAS experiment, *J. Atmos. Oceanic Technol.*, *20*(10), 1375–1387.
- Quinn, P. K., D. J. Coffman, V. N. Kapustin, T. S. Bates, and D. S. Covert (1998), Aerosol optical properties in the marine boundary layer during the First Aerosol Characterization Experiment (ACE 1) and the underlying chemical and physical aerosol properties, *J. Geophys. Res.*, *103*(D13), 16,547–16,563.
- Reid, J. S., H. H. Jonsson, M. H. Smith, and A. Smirnov (2001), Evolution of the vertical profile and flux of large sea-salt particles in a coastal zone, *J. Geophys. Res.*, *106*(D11), 12,039–12,054.
- Sievering, H., B. Lerner, J. Slavich, J. Anderson, M. Posfai, and J. Cainey (1999), O₃ oxidation of SO₂ in sea-salt aerosol water: Size distribution of non-sea-salt sulfate during the First Aerosol Characterization Experiment (ACE 1), *J. Geophys. Res.*, *104*(D17), 21,707–21,717.
- Sievering, H., J. Cainey, M. Harvey, J. McGregor, S. Nichol, and A. P. Quinn (2004), Aerosol non-sea-salt sulfate in the remote marine boundary layer under clear-sky and normal cloudiness conditions: Ocean-derived biogenic alkalinity enhances sea-salt sulfate production by ozone oxidation, *J. Geophys. Res.*, *109*, D19317, doi:10.1029/2003JD004315.
- Stevens, B., et al. (2003), Dynamics and chemistry of marine stratocumulus: Dycoms-II, *Bull. Am. Meteorol. Soc.*, *84*(5), 579–593.
- Swietlicki, E., et al. (2000), Hygroscopic properties of aerosol particles in the northeastern Atlantic during ACE-2, *Tellus, Ser. B*, *52*(2), 201–227.
- Tang, I. N., A. C. Tridico, and K. H. Fung (1997), Thermodynamic and optical properties of sea salt aerosols, *J. Geophys. Res.*, *102*(D19), 23,269–23,276.
- Twomey, S. (1968), On the composition of cloud nuclei in the northeastern United States, *J. Rech. Atmos.*, *3*, 281–285.
- Van Dingenen, R., F. Raes, J. P. Putaud, A. Virkkula, and M. Mangoni (1999), Processes determining the relationship between aerosol number and non-sea-salt sulfate mass concentrations in the clean and perturbed marine boundary layer, *J. Geophys. Res.*, *104*(D7), 8027–8038.
- Warneck, P. (1988), *Chemistry of the Natural Atmosphere*, *Int. Geophys. Ser.*, vol. 41, 757 pp., Elsevier, New York.
- Wiedensholer, A. (1988), An approximation of the bipolar charge distribution for particles in the submicron size range, *J. Aerosol Sci.*, *19*(3), 387–389.
- Woodcock, A. H. (1950), Sea-salt in a tropical storm, *J. Atmos. Sci.*, *7*(6), 397–401.
- Yoon, Y. J., and P. Brimblecombe (2002), Modelling the contribution of sea salt and dimethyl sulfide derived aerosol to marine CCN, *Atmos. Chem. Phys.*, *2*, 17–30.
- Zhou, J. C., E. Swietlicki, O. H. Berg, P. P. Aalto, K. Hameri, E. D. Nilsson, and C. Leck (2001), Hygroscopic properties of aerosol particles over the central Arctic Ocean during summer, *J. Geophys. Res.*, *106*(D23), 32,111–32,123.

A. D. Clarke and J. Zhou, School of Ocean and Earth Science and Technology, University of Hawaii, 1000 Pope Road, Honolulu, HI 96822, USA. (tclarke@soest.hawaii.edu)

S. R. Owens, Department of Meteorology, University of Hawaii, 2525 Correa Road, HIG 350, Honolulu, HI 96822, USA.